Research Article

Direct 3D Printing of Highly Anisotropic, Flexible, Constriction-Resistive Sensors for Multidirectional Proprioception in Soft Robots

Saeb Mousavi, David Howard, Fenghua Zhang, Jinsong Leng, and Chun H. Wang*

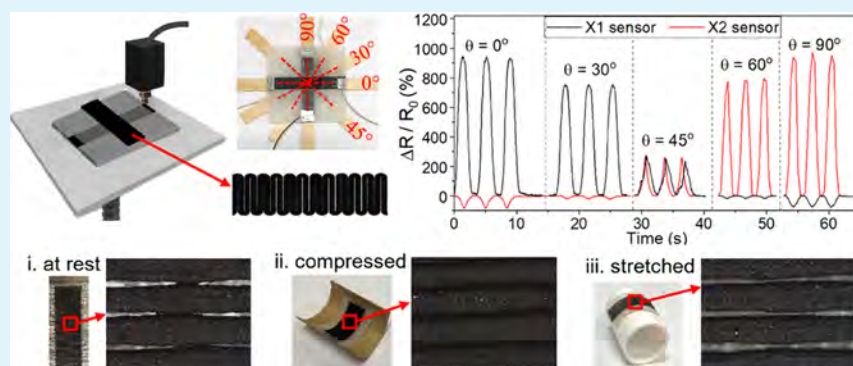Cite This: *ACS Appl. Mater. Interfaces* 2020, 12, 15631−15643

Read Online

ACCESS | Metrics & More | Article Recommendations | Supporting Information

ABSTRACT: A key missing technology for the emerging field of soft robotics is the provision of highly selective multidirectional tactile sensing that can be easily integrated into a robot using simple fabrication techniques. Conventional strain sensors, such as strain gauges, are typically designed to respond to strain in a single direction and are mounted on the external surface of a structure. Herein, we present a technique for three-dimensional (3D) printing of multidirectional, anisotropic, and constriction-resistive strain sensors, which can be directly integrated into the interior of soft robots. Using a carbon-nanotube-reinforced polylactic acid (PLA-CNT), both the sensing element and the conductive interconnect of the sensor system are 3D-printed. The sensor's sensitivity and anisotropy can be adjusted by controlling the air gap between printed adjacent tracks, infill density, and build orientation relative to the main loading direction. In particular, sensors printed with a near-zero air gap, i.e., adjacent tracks forming a kissing bond, can achieve a gauge factor of ∼1342 perpendicular to the raster orientation and a gauge factor of ∼1 parallel to the raster orientation. The maximum directional selectivity of this ultrasensitive sensor is 31.4, which is approximately 9 times greater than the highest value reported for multidirectional sensors so far. The high sensitivity stems from the progressive opening and closing of the kissing bond between adjacent tracks. The potential of this type of sensors and the simple manufacturing process are demonstrated by integrating the sensor with a soft robotic actuator. The sensors are able to identify and quantify the bending deformation and angle in different directions. The ability to fabricate sensors with tailored footprints and directional selectivity during 3D printing of soft robotic systems paves the way toward highly customizable, highly integrated multifunctional soft robots that are better able to sense both themselves and their environments.

KEYWORDS: *3D printing, multidirectional tactile sensor, anisotropy, constriction-resistive strain sensor, printing density, directional selectivity, soft robotics*

■ INTRODUCTION

A major paradigm shift in robotics is from the current usage of rigid bodies assembled from discrete sensing, actuation, and structural units to the construction of soft robots. Soft and flexible robots are set to revolutionize many domains, including healthcare, disaster response, and collaborative industries. Recent developments in the field of additive manufacturing have helped soft robotics to progress toward creating integrated, multifunctional, deformable structures that couple sensing, actuation, and structure.[1] One key to realizing these goals is the ability to integrate sensors directly into the soft robotic structures to detect posture and motion in multiple

directions (state estimation). State estimation is particularly challenging as soft robots undulate, bend, and flex in different directions during operation; as such, the sensors have to be able to measure those movements while undergoing large deformation alongside the robot. In addition, robots need to

sense unforeseen deformations in the body brought about by (i) unintended changes in posture caused by the robot responding to new stimuli and (ii) environmental collisions. Multidirectional motion sensing is therefore critical to enable a soft robot to understand its current state and therefore react appropriately.

Currently, multidirectional tactile sensors are still in their infancy. Strain gauges have previously been studied, but they typically operate in one direction only, so multiple strain gauges are needed to determine a three-dimensional (3D) strain state. Din et al.[2] designed a stretchable multidirectional capacitive sensor system composed of three separate sensors with small cross-sensitivity for distinguishing between normal, shear, and axial loads. Park et al.[3] proposed a system of four strain gauges, each sensitive only to the strain applied in one particular direction, as a multidirectional strain monitoring system. Ridzuan et al.[4] proposed a tooth-inspired tactile sensor system composed of four sensors surrounding a central rod, which serves as an actuator. The sensory system compares the output of four strain gauges to predict the bending angle of a rod actuator. Another method to achieve multidirectional tactile sensing involves the spatial distribution of multiple electrodes over a sensing body.[5−8] By comparing the outputs of several pairs of electrodes, one can calculate the location and direction of a given applied load. Lee et al.[5] used this method to detect the loading direction on a soft piezoresistive surface of a poly(dimethylsiloxane) (PDMS)−multiwall carbon nanotube (MWCNT) composite. By imprinting poly(vinylidene fluoride) (PVDF) on an array of four electrodes, Chen et al.[6] demonstrated the application of multielectrode, multidirectional tactile sensing. The main drawbacks of this method are excessive electrode wirings and a complex fabrication process. It is of great importance to achieve multidirectional strain detection using a single sensor so as to reduce the construction complexity and improve spatial resolution. In this regard, Pang et al.[9] introduced an interlocking-based strain sensor using metal-coated, high-aspect-ratio polyurethane-based nanofibers. The sensor's sensitivity varies considerably with the mode of loading, such as pressure, shear, and torsion, and therefore offers some potential as a multidirectional sensor, should the multiple stimuli occur sequentially. Similar interlocking techniques were used later by Park et al.[10,11] and then Boutry et al.[12] to fabricate multidirectional tactile sensors with similar reported performances. More recently, Van Meerbeek et al.[13] employed machine learning techniques to enable a soft actuator integrated with optical fiber sensors and fabricated through soft lithography, to predict whether it was twisted clockwise, twisted counterclockwise, bent up, or bent down. The common issue with these techniques is their complex geometrical design and the associated manufacturing challenges, which limits their general applicability.

Recently, 3D printing of soft tactile sensors and actuators has attracted huge attention due to the numerous advantages of additive manufacturing, such as facile integration of multiple materials into a complex 3D structure without producing any waste material.[14−16] Three-dimensional printing curable polymer resins as tactile sensors with good sensitivity and recovery have been reported by several researchers.[17−28] Unlike soft physical sensors that were developed using thermoset polymers such as PDMS, tactile sensors made of thermoplastics are considerably simpler and quicker to print as they do not need any postprocessing to cure. Tactile sensors have been 3D-printed using stretchable thermoplastic-based

composites with piezoresistive carbon nanostructure (CNS) networks,[28−32] but these sensors tend to have a low sensitivity, with the maximum sensitivity being reported to be around 80. The reported sensors to date are also isotropic and lack the ability to identify deformation in different directions. By choosing a more rigid polymer matrix, such as polylactic acid (PLA), we previously reported a highly sensitive thermoplastic PLA−graphene sensor based on a fragmentation mechanism.[33] The sensor showed a gauge factor of ∼550, but it lacked the multidirectional strain-sensing capability.

Engineering appropriate anisotropic structures as multidirectional tactile sensors is emerging as a novel approach. This method has been used both for improving the sensitivity in a particular direction[34,35] and for multidirectional strain sensing.[35−39] Due to the anisotropic microstructure of aligned conductive materials, the sensors show different sensitivities parallel and perpendicular to the alignment direction. In this regard, Chen et al.[40] proposed a multidirectional bending and pressure sensor made of two orthogonal carbon nanotube−polyurethane sponge strips (CPSSs), each of which has a different sensitivity when bent or pressed. Mu et al.[41] developed a tactile sensor that enables the detection of both normal and tangential forces, with specific opposite resistance-changing outputs using two sublayered carbon nanotube (CNT)/graphene oxide (GO) hybrid 3D conductive networks that were anchored on a thin porous PDMS layer. Sui et al.[38] reported a directional sensor based on flexible, aligned CNT film nanocomposites. Also, Lee et al.[39] reported a stretchable multidirectional strain sensor based on highly aligned, anisotropic carbon nanofiber films via the electrospinning technique. Although these works show the usage of anisotropy in achieving directional selectivity for a strain sensor, they are not suitable for 3D printing and require a rather complex fabrication process with little or no control of the anisotropic structure. Herein, we present a facile technique for creating a highly sensitive and multidirectional printed anisotropic tactile (PAT) sensor using a carbon-nanotube-reinforced polylactic acid (PLA-CNT) composite. To characterize the performance of the PAT sensor under large deformation, a sandwich design is selected where a thermoplastic polyurethane (TPU) filament and a PLA-CNT filament are fed into a fused deposition modeling (FDM) printer to fabricate a PLA-CNT sensor encapsulated between two TPU layers. The PLA-CNT nanocomposite is the constriction-resistive sensing material, while the stretchable TPU is employed to insulate the sensing element.

The anisotropic structure of this 3D-printed sensor shows significantly different sensitivity to bending applied in different directions and makes it possible to identify multidirectional bending deformation. The sensor performance is characterized by direct stretching and bending tests. Results reveal that the sensor has high sensitivity, excellent recovery, and very stable response to cyclic loading and is capable of differentiation of multidirectional deformation, thus enabling the determination of the direction and degree of bending, which is particularly important for soft robotic applications.

Furthermore, we show that the 3D printing technique can be extended to construct stretchable conductors for signal transmission. Inspired by the success of wavy and helical patterns as stretchable conductors,[42−45] we demonstrate that stretchable conductors can be 3D-printed using the same CNT-reinforced PLA by selecting a large air gap between adjacent tracks. To demonstrate the practical benefits of this
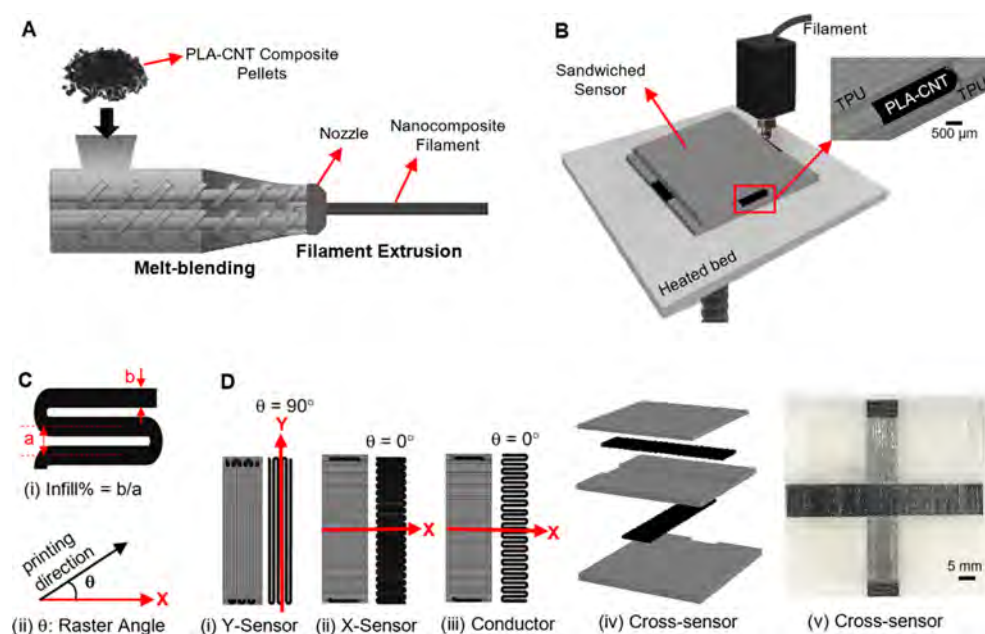
Figure 1. Step-by-step process of fabricating the PAT sensors. (A) PLA pellets and CNT nanofillers are first solution-mixed and then fed into a twin-screw extruder with continual melt-mixing. A filament is extruded through a nozzle at the end of the extruder. (B) Extruded filament together with the TPU filament is then used to 3D-print sandwiched sensors. (C) Illustrative definition of (i) the infill density/ratio of the 3D-printed sensor layer as the ratio between the track width and the track spacing, and (ii) raster angle (θ) of 3D printing. (D) Schematics of different types of printed sensors: (i) Y-sensor with a raster angle of 90°, (ii) X-sensor with near-zero air gap between tracks and a raster angle of 0°, (iii) conductor printed with large air gaps between tracks and a raster angle of 0°, (iv) cross-sensor consisting of two X-sensors placed in orthogonal directions sandwiched between TPU layers, and (v) image of a printed cross-sensor.

new type of 3D-printable sensors, two soft robotic actuators with integrated sensors were manufactured by the same FDM machine. The results show that the ability to integrate structural, conducting, and sensing materials into one 3D-printed part offers several advantages (e.g., customizable footprint and performance and simple fabrication), overcomes some of the limitations of conventional fabrication methods, and thus opens new opportunities for 3D printing of soft robots with integrated tactile sensors.

■ RESULTS AND DISCUSSION

Fabrication of PAT Sensors. The step-by-step process of fabricating the PAT sensors is shown in Figure 1. In this work, the PLA-CNT nanocomposite was chosen to serve as the sensing material for the sensor. To fabricate the sensing layer, PLA pellets and CNT were dissolved in dichloromethane ($CHCl_2$) solvent and then dried at room temperature to obtain the PLA-CNT composite with a CNT mass fraction of 12%. Then, the composite material was cut into pieces and extruded using a twin-screw extruder (Figure 1A) to make filaments, which were then used to 3D-print the sensor. Although PLA is a relatively stiff material at room temperature, previous research on tactile sensors that have been 3D-printed using stretchable thermoplastic-based composites with piezoresistive carbon nanostructure (CNS) networks[28−32] has found that the sensors had low sensitivity, with the maximum sensitivity of 80. In this work, carbon-nanotube-reinforced PLA was chosen to 3D-print constriction-sensitive sensors, utilizing a novel kissing-bond mechanism. The resultant sensors were proven to be highly flexible and sensitive.

PLA filaments with different CNT contents of 5, 8, 12, and 14 wt % were synthesized to identify the optimum CNT loading that allows fused filament fabrication and gives the highest electrical conductivity. By comparing the electrical conductivities of these filaments with those reported in the literature (see Figure S1), it is clear that the loadings used in this study are above the percolation threshold of CNT-reinforced PLA. The conductivity values of the filaments fabricated with different CNT contents are listed in Tables S1−S3 in the Supporting Information. Five specimens were tested with each CNT content. The results show that the higher the CNT content, the higher the electrical conductivity. However, when the CNT content exceeded 12 wt %, the material became rather brittle and was not suitable as a feedstock filament for continuous fuse deposition modeling printers (see Figure S2A,B for stress−strain curves of the filaments with 12 and 14 wt % CNT contents, respectively). Therefore, PLA filaments with 12 wt % CNT content were chosen for sensor fabrication. At this loading, the PLA-CNT filament shows a conductivity of ~149 S/m and a failure strain of ~3.2%. To make the sensor robust in challenging environments, such as making contact with and rubbing against other objects, the sensor was first printed onto a TPU substrate and then another TPU skin was printed on top of it to provide a good protection, as shown in Figure 1B.

Three-dimensional printing makes it possible to rapidly vary several printing parameters to alter the properties of the sensors during the printing process. The most important parameter here is the infill ratio, which is defined as b/a, where b is the width of the printed tracks and a is the spacing between two neighboring tracks (see Figure 1C). The sandwich PAT sensor was fabricated using an extremely simple FDM 3D printing technique. Three types of demonstrator sensors and a conductor were fabricated as shown in Figure 1D. The X- and Y-sensors served to characterize the sensor's performance in the lateral and
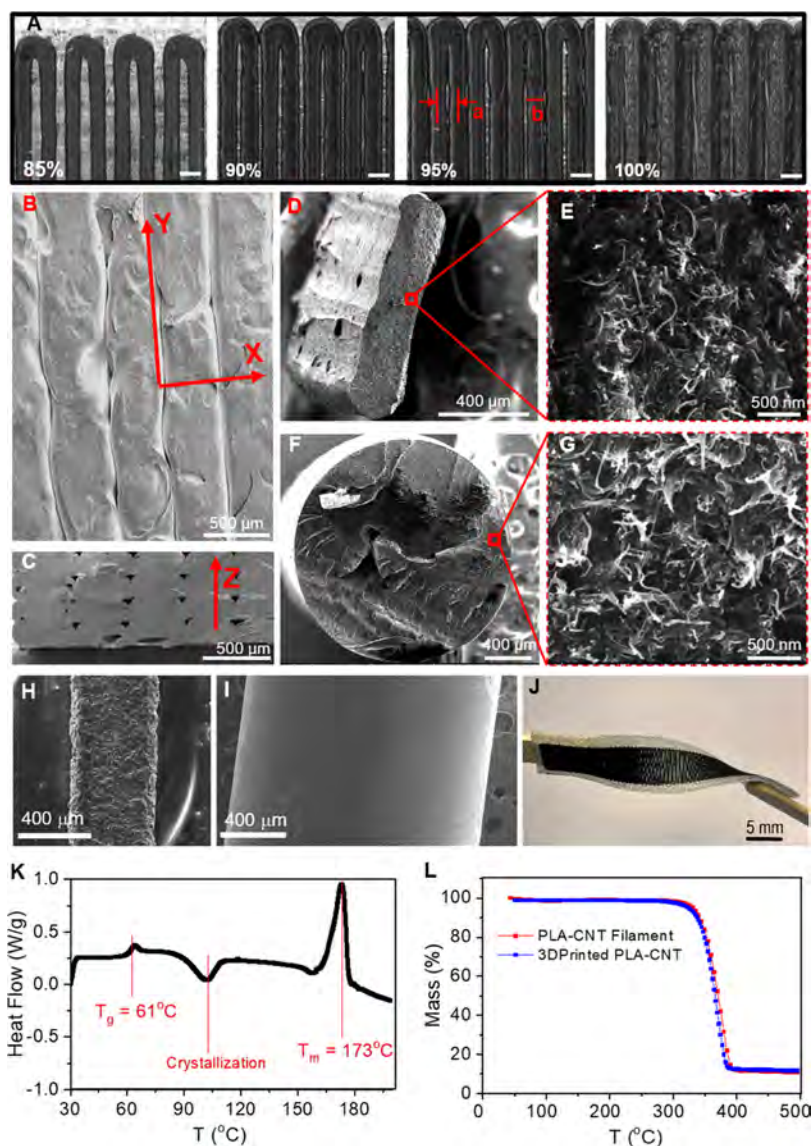
Figure 2. Microstructure and thermal characterization of the sensor materials. (A) Microscopic images of the PLA-CNT sensors with different infill densities (85, 90, 95, and 100%) 3D-printed on TPU. The actual infill density (b/a) is different from nominal infill densities shown in these figures. The scale bars are 500 μm. Scanning electron microscopy (SEM) images of (B) top view and (C) fractured cross-sectional view of the 3D-printed TPU (95% infill density). (D) Low-magnification and (E) high-magnification cross-sectional SEM images of two tracks of PLA-CNT 3D-printed with 100% infill density. (F) Cross section of the PLA-CNT filament and (G) high magnification of (F). To compare the surface roughness, top-view surface images of (H) PLA-CNT track 3D-printed on TPU and (I) PLA-CNT filament were taken without platinum coating. (J) Picture of the 95% infill X-sensor without top TPU layers showing the flexibility of the sensor under twisting. (K) Differential scanning calorimetry (DSC) test result of the PLA-CNT filament. The DSC test shows the glass transition (T_g) and melting (T_m) temperatures of 3D-printed PLA-CNT filaments. (L) Thermogravimetric analysis (TGA) test result of the PLA-CNT filament confirms that the CNT concentration in the PLA matrix is ~12%.

longitudinal directions, respectively. A low-density X-sensor was fabricated to serve as a conductor due to its extremely low sensitivity to deformation, and a combination of two X-sensors in the form of a cross-sensor provided the PAT sensor with a multidirectional functionality. Full printing parameters for printing the sensors and conductor can be found in Table S4 in the Supporting Information.

Altering the infill ratio affects the level of contact between adjacent printed tracks and therefore changes the resistance of the printed sensor. In particular, changing the infill ratio affects the strength of the kissing bond between adjacent tracks, thus altering the anisotropic structure of the sensor. In this way, X-sensors can be designed to feature significantly different

sensitivities to deformation along and perpendicular to the sensor's raster direction, giving the sensors a multidirectional sensing ability.

To characterize the effect of the infill ratio on sensors' performance, both X-sensors and Y-sensors with nominal infill ratios of 100, 95, 90, and 85% were 3D-printed and tested. It should be noted that while these nominal printing density values were set in the printer software, they may differ from the actual densities of the printed sensors because the gaps or contact conditions between printed tracks are affected by parameters such as material properties (e.g., viscosity), the bed temperature, and the printing speed. In the present case, the nominal infill densities of 100, 95, 90, and 85% result in actual
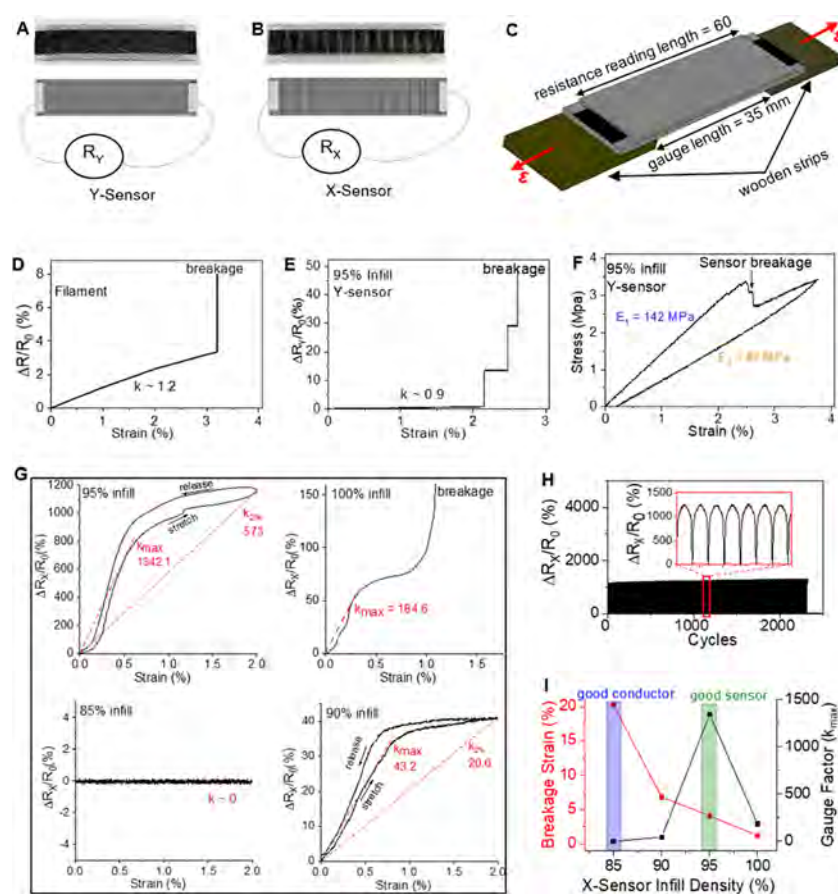
Figure 3. Electromechanical performance of the filament and X- and Y-sensors. The pictures and schematics of (A) Y-sensor and (B) X-sensor with electrical wiring. (C) Sensors were glued at the back on two wooden strips for tensile tests. The sizes are in millimeters. Strain-sensing performance of (D) PLA-CNT filament and (E) 95% infill Y-sensor. (F) Stress−strain curve of 95% infill Y-sensor showing the sensing layer's mechanical breakage point. (G) Tensile sensitivity tests of X-sensors with 100, 95, 90, and 85% infill densities, with maximum gauge factors and gauge factors at ε = 2% shown on each graph. (H) Cyclic tensile sensitivity test with 95% infill X-sensor (ε = 2%) showing the durability of the sensor. (I) Comparison of strain at sensor breakage with maximum gauge factor for X-sensors with different printing densities.

infill densities of 105% (slight overlapping of adjacent tracks), 92.75% (kissing bond), 77.7% (weak kissing bond), and 58.8% (no bonding between adjacent tracks), respectively (for more details, see Figure 2A and the infill analysis in SupportingInformation). For consistency with printer settings, hereafter, we refer only to the nominal infill densities.

Optical, Thermal, and Mechanical Analyses. Optical images of the PLA-CNT conductor (85% infill density) and sensors (90, 95, and 100% infill densities) printed on a TPU substrate are shown in Figure 2A. SEM images of the top and cross-sectional views of the 3D-printed TPU layers are shown in Figure 2B,C, respectively. TPU was printed with 95% infill density, effectively fusing neighboring tracks together. The low-magnification SEM images of 3D-printed PLA-CNT tracks with 100% infill density (Figure 2D) and the PLA-CNT feedstock filament (Figure 2F) show the cross section of these two materials, while the high-magnification SEM images (Figure 2E,G) confirm the existence of CNT in the polymer matrix. To compare the surface roughness of the extruded strand and the feedstock filament, SEM images of these two materials were taken and are shown in Figure 2H,I. Figure 2J shows a 95% infill X-sensor without a top TPU layer, illustrating the flexibility of the sensor. The results of differential scanning calorimetry (DSC) test of PLA-CNT filaments are shown in Figure 2K, indicating that the glass

transition (T_g) and melting (T_m) temperatures are ∼61 and 173 °C, respectively. Information on the T_g value is useful for choosing a better bed temperature for 3D printing to improve the bonding strength of the sensors with their host structure. This is further discussed in the next paragraph (peel-off tests). The thermogravimetric analysis (TGA) result (Figure 2L) confirms that the CNT content in the PLA matrix is around 12 wt %. PLA starts decomposing at ∼320 °C and is completely decomposed at 400 °C. TGA results also show that the CNT content remains approximately unchanged in the PLA matrix before and after 3D printing, as expected.

The mechanical properties of the PLA-CNT filament and 3D-printed TPU were characterized through tensile testing. The elastic moduli of the PLA-CNT filament and 3D-printed TPU were measured to be 828.0 and 12.6 MPa, respectively as shown in Figure S2A,C. Besides infill density, bed temperature is another important printing variable that can affect the bonding strength of the PAT layer to the TPU and therefore the sensor stretchability and performance. To show the effect of bed temperature on the bonding strength of PLA-CNT with TPU, peel-off tests were conducted on samples printed at different bed temperatures (Figure S2D−F). Results are shown as peel-off load (N) versus displacement (mm). By comparing the peel-off force of two X-sensors printed with 40 and 70 °C bed temperatures (Figure S2E,F), it is evident that the sensor

printed on a 70 °C bed exhibits stronger bonding with the TPU substrate. This can be explained by the difference between the bed temperature and the glass transition temperature of PLA-CNT (T_g = 61 °C). When the bed temperature is raised to 70 °C (above the T_g of PLA-CNT), the printed material remains soft on the bed until the end of the printing process and forms a stronger bonding between tracks and with the TPU substrate. Furthermore, it is noted that the bonding strength of the PLA-CNT/TPU interface is less than that of the TPU/TPU interface. Figure S2G shows the peel-off experimental setup. Optical images of the specimens after the peel-off tests (Figure S2H,I) illustrate the amount of residual PLA-CNT on the TPU surface for the two specimens. SEM characterization of the peeled-off surfaces is shown in Figure S3. Cross-sectional SEM images (Figure S3Ai,Bi) show a gap between the PLA-CNT track and the TPU surface for a sensor printed at a bed temperature of 40 °C, which confirms a weaker bonding. Furthermore, as illustrated in Figure S3Aii,Bii, a sensor printed at a 70 °C bed temperature shows a higher amount of residual PLA-CNT material on the TPU after the peel-off test and therefore confirms a better bonding. Based on the SEM images (Figure S3Aiii,Biii), three regions exist on the TPU surface after the peel-off test in terms of the amount of residual PLA-CNT. Region 1 is where almost no residual material is visible. Region 2 shows some residual material with a small amount of CNTs, and region 3 shows the highest amount of residual materials. These three regions are marked in Figure S3iv−vi, respectively. To evaluate the strain-sensing performance of the X-sensors printed with these two print-bed temperatures, tensile-strain-sensing tests were conducted, and the results are shown in Figure S4. As it is shown, the sensor printed with the 70 °C bed temperature shows considerably higher strain sensitivity. This higher sensitivity is attributed to the improved bonding between the printed PLA-CNT tracks and the TPU substrate, which would suppress disbonding and increase fragmentation. Based on these results, a bed temperature of 70 °C was chosen for printing the sensors in the work described below.

To measure the temperature sensitivity of the sensors, the electrical resistances of the 3D-printed sensors and the filament were recorded in an oven where the temperature was raised at a rate of 10 °C/30 min. The results are shown in Figure S5. Such thermal tests were performed for a PLA-CNT filament, X-sensor, Y-sensor, and a single PLA-CNT extruded track. The results show that the feedstock filament and all of the sensors are largely insensitive to temperature in the range 24−60 °C. The greatest resistance change was ∼0.95% for the X-sensor over a 30 °C temperature variation, which equates to a 0.03% resistance change per 1 °C temperature rise. This excellent temperature insensitivity of the present sensors is very promising as it avoids the need for temperature compensation, as is the case for conventional strain gauges.

Electromechanical Performance. To evaluate the strain-sensing performance of PAT sensors, they were first tested under tensile stretching. The sensor's strain sensitivity or gauge factor, k, is defined as the ratio of the change of electric resistance, ΔR, over the initial resistance R_0 per applied strain ($k = \Delta R/\varepsilon R_0$). The pictures and schematics of Y-sensor and X-sensor with electrical wiring for the measurement of R_y and R_x are shown in Figure 3A,B, respectively. For all of the tensile and bending tests, the sensors were glued to two wooden strips at the two ends, with the electrodes being at the unloaded ends of the sensors to avoid cracks in wire bonding during the

experiments (Figure 3C). The tensile-strain-sensing response of the PLA-CNT filament is shown in Figure 3D and that of a 95% infill Y-sensor in Figure 3E. From Y-sensor's stress−strain curve (Figure 3F), it is noted that the modulus suddenly drops when the sensor layer breaks. The strain sensitivity of the Y-sensor is similar to that of the filament, with a smaller strain at break (∼2.2 versus 3.2%). This lower failure strain can be explained from the higher surface roughness of the extruded PLA-CNT strands (see Figure 2H,I) than that of the feedstock filament, which introduces defects that cause the sensor to break earlier than the filament. In contrast to the filament and Y-sensor, the X-sensor proved to be very sensitive to strain. Tensile sensitivity test results with 100, 95, 90, and 85% infill X-sensors are shown in Figure 3G, including the maximum gauge factors and the corresponding strains. The 95% X-sensor shows an exceptional maximum sensitivity of ∼1342.1 at 0.5% applied strain, which is unprecedented for 3D-printed sensors. Since the 95% sensor exhibits a working range of around 2% strain, the gauge factors of the 90 and 95% sensors at 2% strain, $k_{2\%}$, were calculated to be 573 and 20.6, respectively. These sensors show some hysteresis, which is expected given the viscoelastic nature of TPU. The X-sensor's response to different stretching speeds/frequencies is consistent and is illustrated in Figure S6 in the Supporting Information.

Durability and repeatability are important factors for a sensor, too. As shown in Figure 3H, the X-sensor shows a very good repeatability, with a small drift of 1.4%, and great durability after 2300 cycles of 2% tensile strain. Prior to the cyclic tests, the sensors underwent 3% tensile strain for 20 cycles. A comparison of the breakage strain (sensors are considered broken when the resistance exceeds 100 MΩ) and the gauge factor for X-sensors with different printing densities (Figure 3I) shows that the 95% infill sensor has the highest sensitivity and an 85% infill sensor features the best conductance insensitivity to deformation.

To characterize the multidirectional strain-sensing behavior of the PAT sensor, a cross-sensor consisting of two X-sensors, X1 and X2, with 95% infill density (Figure 4A) was subjected to a tensile strain in 0, 30, 45, 60, and 90° directions. The resistance changes for sensor X1 and sensor X2 (shown in Figure 4B) were determined from the outputs of the two X-sensors as shown in Figure 4C. When a 1% tensile strain was applied to the sensor at 0°, the $\Delta R_x/R_0$ value for sensor X1 increased drastically ($k_x \sim 1300$), while sensor X2 showed a small and negative resistance change ($k_x \sim -79$) due to lateral contraction. When the stretching direction was varied from 0 to 90°, the $\Delta R_x/R_0$ value decreased for sensor X1 and increased for sensor X2. Figure 4D shows the difference of the resistance changes of the two sensors (X1 and X2) versus the stretching direction (θ) and applied strain (ε). To quantify the selectivity of this sensor, Δk (the difference between the maximum k_x and k_y) was plotted against the loading angle, θ (Figure 4E). Selectivity is defined as the magnitude of the gradient ($|\nabla|$) of the best linear fit of Δk versus θ graph.[41,46] Selectivity is a critical performance parameter specific to multidirectional strain sensors, as it measures the ability to distinguish the directions of external loads whereby a higher selectivity means more variation of the output responses as the strain direction changes, which aids the distinction of loading directions.[38] This cross-sensor exhibits a maximum selectivity of 31.4 calculated at 0.5% applied strain, which is much higher than the best value of all stretchable multidirectional strain sensors reported in the literature so far; previously, the highest
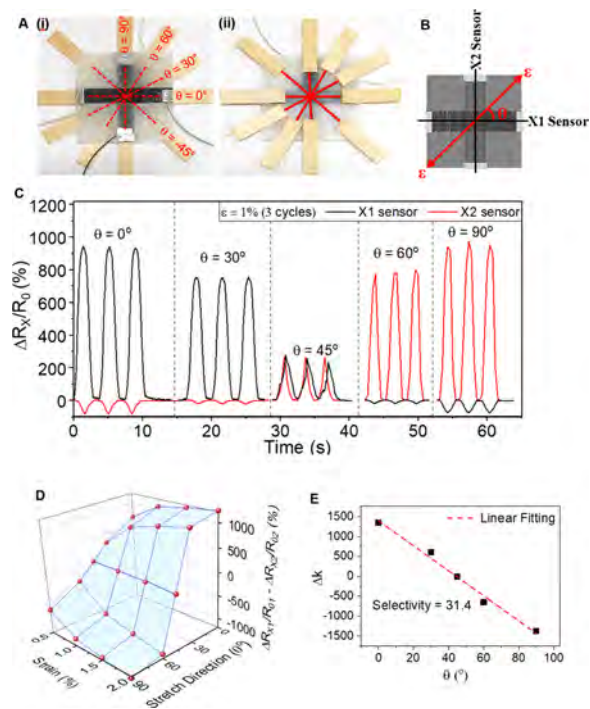
Figure 4. Electromechanical performance of the cross-sensor. (A-i) Front and (A-ii) back pictures of the 3D-printed cross-sensor showing the wooden strips used in tensile tests in different directions. (B) Schematics of a cross-sensor with two X-sensors, namely, X1 and X2, for k_{X1} and k_{X2} calculations. The stretching direction (θ) is also denoted. (C) Tensile strain sensitivity test results in 0, 30, 45, 60, and 90° directions for the 95% infill cross-sensor where a 1% tensile strain was applied for three cycles in each direction. (D) Difference of resistance changes between X1 and X2 sensors plotted versus the applied tensile strain and angle θ. (E) Diagram of Δk ($=k_{X1} - k_{X2}$) versus θ showing the maximum selectivity of the sensor at 0.5% applied strain.

selectivity for a multidirectional strain sensor was reported by Lee et al.[39] with a selectivity of 3.33. The selectivity of the current sensor at 2% strain is 15.9. Table S5 compares the performance of notable multidirectional stretchable sensors reported previously with the current sensor's performance. Based on these findings, our new sensors enable the determination of the magnitudes of applied strains from the measurements of $\Delta R_{X1}/R_{01}$ and $\Delta R_{X2}/R_{02}$. At a given strain, using the $\Delta k-\theta$ plot, one can also calculate the angle (θ) of the principle load/strain experienced by the sensor.

Bending experiments were designed to benefit from the multidirectional behavior of the sensor. The schematic of the cross section of an integrated sensor (Figure 5A) shows the position of the sensing layer with respect to the neutral axis (NA). To limit the tensile strain in the sensor layer when the structure is undergoing bending, the sensor was located close to the neutral axis. The X-sensor and Y-sensor were curved manually around tubes with varying diameters as shown in Figure 5B. Compressive and tensile stretching of the embedded sensor could be easily achieved by reversing the bending of the structure around the tube. The corresponding strain for each tube used in bending tests is shown in Figure 5C. The bending sensitivities of the X-sensors with 85 and 95% infill densities (the best conductor and the best sensor, respectively) are shown in Figure 5D. The 85% infill conductor shows no sensitivity to bending as expected. The 95% infill X-
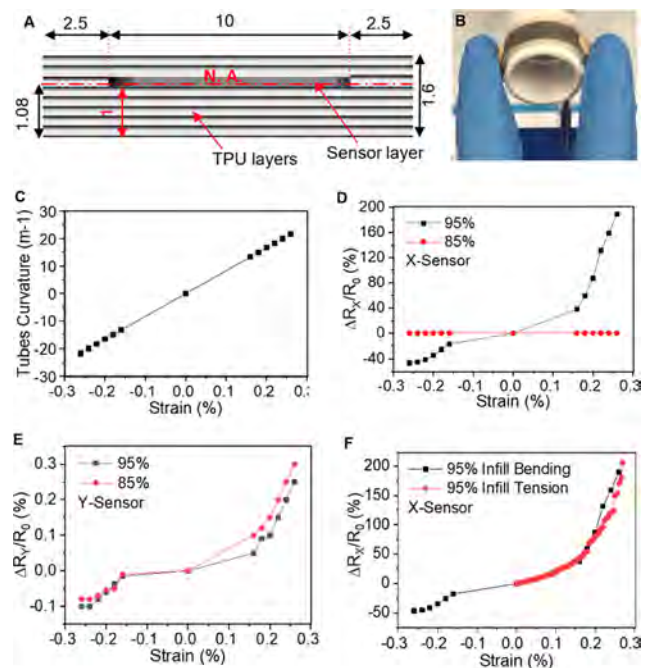
Figure 5. Bending detection tests. (A) Schematics of the cross section of the sensor showing the number of 3D-printed layers. To avoid exceeding the sensing range of sensors, they were placed close to the neutral axis (NA). All of the dimensions are in millimeters. The figure is not to scale. (B) Bending tests done by manually bending the sensor over different tubes with varying curvatures. (C) Calculated strains experienced by the sensors. The bending sensitivities of (D) X-sensor and (E) Y-sensor with 95 and 85% infill densities are measured. (F) Bending test results are consistent with tensile test results in terms of gauge factor.

sensor shows a high sensitivity, which is consistent with the tensile test results. Furthermore, the Y-sensors exhibit extremely lower sensitivities to bending as shown in Figure 5E, and this is expected from their tensile characteristics. The values of resistance changes calculated from bending tests are validated through comparison to the tensile test results (Figure 3G) as shown in Figure 5F. This performance confirms the suitability of the sensor as a flexing/bending sensor.

Sensing Mechanism of the PAT Sensors. As discussed in previous sections, the anisotropic structure of our PAT sensor gives rise to its multidirectional strain-sensing characteristics. This anisotropy is achieved by controlling the raster direction, infill ratio, and bed temperature in 3D printing. The strain sensitivity is achieved through an abrupt change of the constriction resistance level. When two conducting materials are joined, the true area of contact at the interface determines the true cross section through which the electronic flow occurs. As illustrated in Figure 6A, the flow of electrons through these narrow areas causes an increase in resistance, which is known as constriction resistance.[47] Accordingly, one can design sensors of high sensitivity using materials that have very low intrinsic sensitivity by engineering the microstructure such that the geometry of contact changes with deformation, which in turn significantly changes the electric resistance. In this study, by adjusting the infill density, it is possible to tune the bond strength of adjacent tracks from a strong bond to a weak or kissing bond. Specifically, when the infill density is around 90%, neighboring tracks form a kissing bond after printing. The weakly bonded tracks would progressively separate under
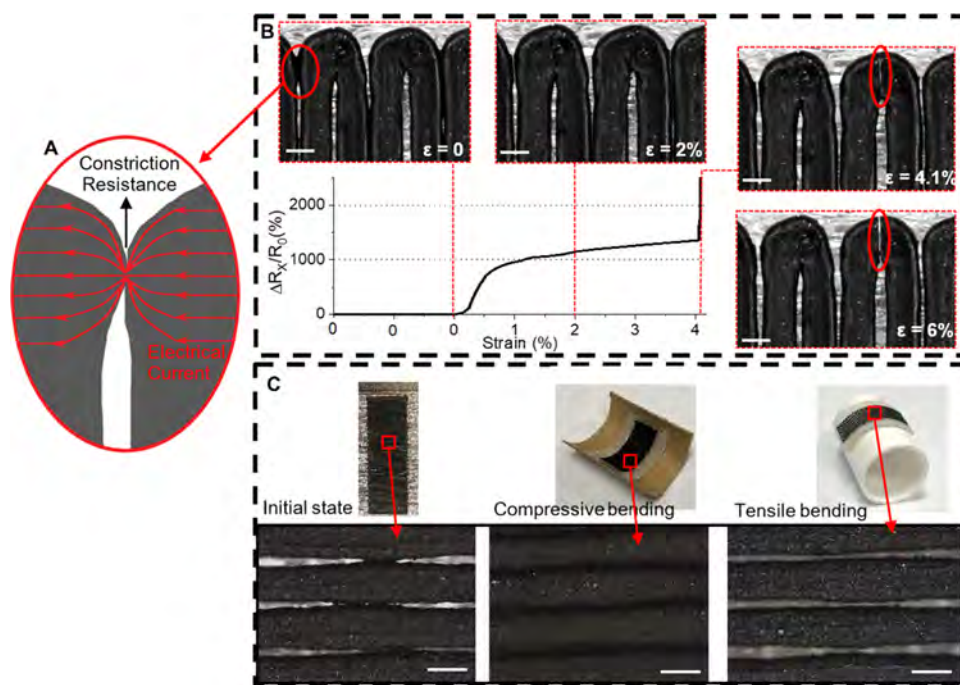
Figure 6. Sensing mechanism of the PAT sensors. (A) Schematic of two neighboring 3D-printed PLA-CNT tracks showing the electrical current flow through a kissing bond, which creates constriction resistance. (B) Microscopic images of a 95% X-sensor shown under different tensile strains and the plot of corresponding resistance changes. The resistance of the sensor changes drastically due to the change of effective contact area between neighboring printed tracks. Sensor failure occurred when the curved segment linking the parallel tracks cracked. (C) Microscopic images of a 90% X-sensor shown under compressive and tensile bending strains. In compression, the neighboring lines close up the gap and reduce the resistance, and in tension, the connected lines fragment and open up to increase the resistance. All of the scale bars are 400 μm.

strain, giving rise to a rapid increase in electric resistance with strain. The results show that this phenomenon is the most significant in a 95% sensor compared to sensors printed at 90% infill ratio; the infill ratio of 100% gives a complete overlap and very strong bond and is hence not suitable for printing sensors. A full microscopic characterization of the X-sensors under tensile deformation is presented in Figure S7 in the Supporting Information. As shown in this figure, the 95% infill X-sensor undergoes a fragmentation process, which results in a dramatic increase of its resistance when stretched. In contrast, the 85% infill X-sensor does not fragment and acts more like a conductor up to a high strain (~20%). The sensing mechanism under tensile stretching for a 95% infill X-sensor is illustrated in Figure 6B and in Video S1 in the Supporting Information as well.

To assess the repeatability of the results obtained with the 95% infill X-sensor, ten specimens with the same printing conditions and parameters were fabricated and their sensing performances measured and compared. As shown in Figure S8 in the Supporting Information, their sensitivity is in a similar range, with an average of 538.34 and a coefficient of variation of 7.58%.

The same sensing mechanism exists in bending and tensile actuations. When the sensor is stretched during a tension (or in tensile bending as shown in Figure 6C), the weak connection between tracks will be disrupted, leading to a rapid increase in resistance. During a compressive bending, the tracks will be forced closer together and make better contact; as a result, the cross section available for electrical current passage will increase, leading to a rapid drop in the sensor's resistance. In contrast, bending in the Y direction does not significantly affect the connection between sensor tracks;

therefore, a much lower sensitivity was observed. The X-sensors show a higher stretchability than the Y-sensors printed with the same infill ratio. This is because the X-sensors fail when cracking occurs in the curved segment linking the long parallel tracks, as illustrated in Figure 6B. For Y-sensors, sensor failure corresponds to the cracking of the long parallel tracks. Since the curved segment is much shorter than the long parallel tracks, a higher strain is needed to cause them to crack compared to the parallel tracks.

Applications of the PAT Sensor in Soft Robotics. Due to its low compliance, a soft robot's internal posture can change in the presence of internal and external loads, which may be unknown. To keep track of the 3D posture of a soft robot to allow for effective control, it is important to develop a method to give a soft robot a sensing ability such that it can detect its own posture and movements in different directions. Although many novel mechanisms and materials have been developed for soft robots,[48,49] the development of cheap and widely applicable methods of sensorizing soft structures so that they can accurately estimate their own posture remains a challenge. Besides sensing for state estimation, flexible conductors are also required to transmit sensor signals around the robot's body to the processor. By printing at 95% infill and 85% infill densities, we can integrate sensors and conductors to fabricate multifunctional sensor−conductor−actuator systems by fused deposition modeling. To demonstrate this new approach, two types of actuators were 3D-printed. First, a four-armed highly porous actuator with an internal infill density of 10% was 3D-printed (Figure 7A), and then, the X1 and X2 sensors (95% infill) and conductors (85% infill) were printed on the actuator. In the last step, a covering layer of TPU was 3D-printed to encase the sensors and conductors as shown in
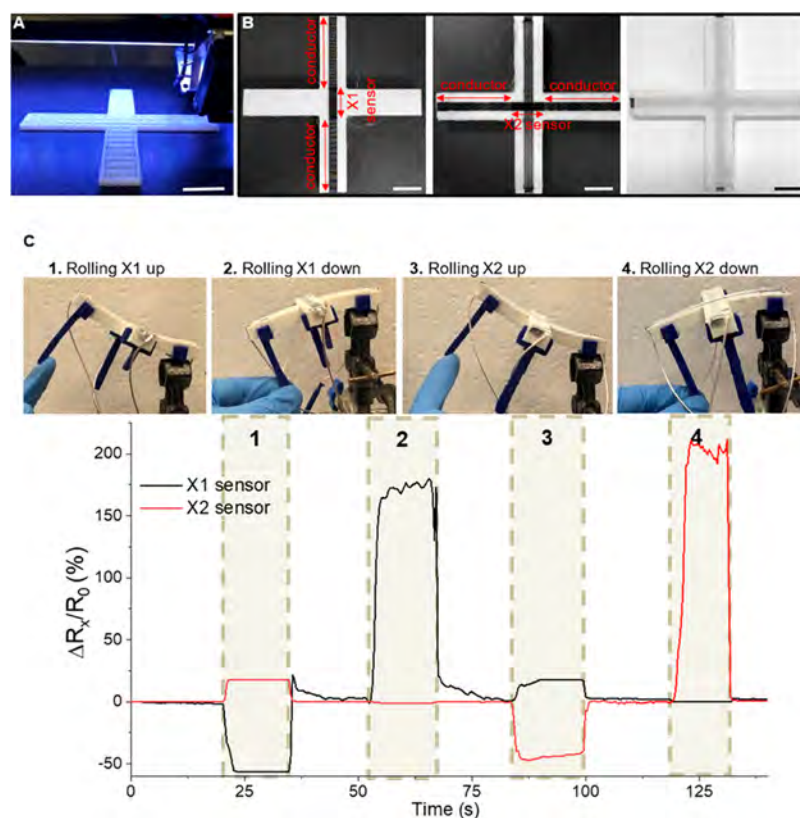
Figure 7. Demonstration of the multidirectional rolling detection. (A) Picture of the porous (low-infill) four-armed actuator while being 3D-printed. (B) Steps of embedding the cross-sensors (X1 and X2 sensors) and conductors into the actuator. All of the scale bars are 15 mm. (C) Four types of actuations were applied to the actuator: (1) rolling up in the direction of the X1 sensor, (2) rolling down in the direction of the X1 sensor, (3) rolling up in the direction of the X2 sensor, and (4) rolling down in the direction of the X2 sensor. The cross-sensor can clearly distinguish whether it is being rolled up or down and whether it is rolling in X1 or X2 directions. This behavior of the cross-sensor proves its capability for multidirectional bending detection.

Figure 7B. Videos S2 and S3 (Supporting Information) show how the conductors and X1 sensor were printed on the actuator, respectively. As illustrated in Figure 7C, by measuring the output resistances of X1 and X2 sensors, one can easily distinguish whether the actuator is rolling up or down and whether it is rolling in X1 or X2 directions. This proof-of-concept demonstration proves that this sensor can be used in more complex actuator systems for the purpose of multidirectional bending detection.

As a second demonstration, a sensor was used for the detection of bending in a two-armed pneumatic actuator gripper. First, the actuator (Figure 8A) was 3D-printed, and then, two 85% conductors and a 95% X-sensor were printed on the side of the actuator (Figure 8B). By printing the sensor around the neutral axis of the system, the sensor was able to function under large deformation without breakage. As shown in Figure 8C,D, the sensor successfully detected the bending direction and magnitude. More details of this demonstration can be found in the Videos S4 and S5 (Supporting Information).

To assess the accuracy of the new sensors, the signal-to-noise ratio (SNR) was calculated for the sensor−conductor−actuator system.[50] SNR is defined as the sensor signal amplitude divided by the noise amplitude[50]

$$SNR = avg(\Delta R)/\sigma_{baseline}$$

where $avg(\Delta R)$ is the average resistance change calculated under strain and $\sigma_{baseline}$ is the standard deviation of the

baseline resistance.[51] Detection of a deformation event typically requires a minimum of 6 dB (signal strength being twice the noise or SNR = 2).[52] A high SNR is desirable for the reliable measurement of the small strain differentials.[53] The SNR for the 95% infill X-sensor under 1% strain is about 82 000, implying that the present sensor is capable of resolving strain as small as 0.25 microstrain. For the sensor−conductor system shown in Figure 8C, the calculated SNR value is 66.7 when the bending angle is 7°, meaning that this sensor can detect a minimum bending angle of 0.2° at SNR = 2. For more details on calculations of the SNR values, see Table S6 and Figures S9, S10 in the Supporting Information.

■ CONCLUSION

We have developed novel designs for multidirectional tactile sensors and conductors that can be readily 3D-printed using a fused deposition modeling technique. The printed sensors have very high sensitivity with strain gauge factors ($k \sim 1342$) and high selectivity (31.4). This high sensitivity stems from the strong constriction-resistive response of the printed tracks with a weak or kissing bond to deformation under tension and compression. By designing a kissing-bond geometry, we have demonstrated flexible sensors with very high gauge factors using a material with very low intrinsic piezoresistivity (PLA-CNT nanocomposite). With different sensitivities to tension and compression, the sensors can distinguish tensile and compressive bending, making it possible to differentiate bending directions.
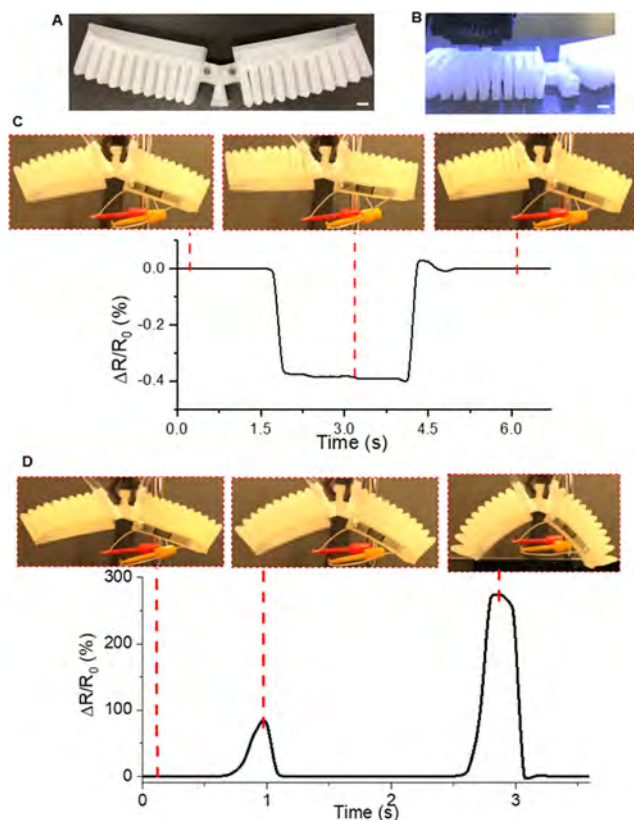
Figure 8. Demonstration of the bending detection with a soft pneumatic gripper. (A) Actuator was 3D-printed and then (B) sensor and conductors were 3D-printed on the surface of the actuator. Both the scale bars are 10 mm. (C) Demonstration of the sensor response in the deflation/vacuum state (bending upward). (D) Demonstration of the sensor response in inflation with different bending magnitudes (bending downward). The pictures show the actuator's different statuses at each sensor resistance reading.

The infill ratio has been found to play a critical role in deciding whether a printed layer functions as a highly sensitive sensor or an excellent electrical conductor. In addition, a cross-sensor consisting of two sensing elements has a very high selectivity of 31.4, which is ~9 times the highest value reported in the literature and makes it suitable as a multidirectional strain sensor.

The new sensors can be fabricated by a simple FDM 3D printing process and have been found to be durable under repeated tensile stretching. The limitation of the current sensors is their low stretchability because of the intrinsic low ductility of the sensing material containing high loading of carbon nanotubes (PLA with 12 wt % CNT). This limitation can be mitigated by placing the sensor layer near the neutral axis of a bending component during the 3D printing process. This research paves the way for the use of low-cost and widely accessible techniques to enable state estimation and effective control of soft robotic systems. The ability to directly 3D-print flexible conductive interconnects offers a major new route to embedding electronics for signal transmission. Three-dimensional printing and integration of sensors and conductors in soft robots open up new opportunities for multifunctional intelligent soft robots and bypass some of the major limitations of conventional fabrication methods, such as the problem of mounting the sensors on the actuator and making the sensors fully conform to a complex surface.

EXPERIMENTAL SECTION

Fabrication of the PLA-CNT Filament. TPU Ninjaflex filament (from NinjaTek) was purchased and used without further processing for printing the actuator and sensors. For fabrication of the PLA-CNT filament, first, PLA pellets (provided by Harbin Institute of Technology) and CNT (TNIM4, Chengdu Organic Chemicals Co. Ltd.) were dissolved in dichloromethane ($CHCl_2$) solvent and then dried at room temperature to obtain the PLA-CNT composite with a CNT mass fraction of 12%. Then, the composite material was extruded using a twin-screw extruder (CTE 20, Coperion Nanjing Machinery Co., Ltd).[54] The PLA-CNT composite filament was extruded in six extrusion temperature zones set at 175, 175, 175, 175, 175, and 180 °C. After that, the composite filament went through a cooling system and a tracking device to make the filament with 1.75 ± 0.5 mm diameter.[55]

Three-Dimensional Printing of the Sensors and Conductor. The 3D-printed sensor consists of a sensing element made of the PLA-CNT composite encased within TPU. A 3DGence FDM printer was used for printing the sensors and actuator. For printing the sensors, first, a substrate of TPU with a thickness of 1.2 mm was printed. The surface of this substrate was designed to contain a slot in the shape of the sensing layer (PLA-CNT). After printing the substrate, the nozzle and filament were changed, and the printer was loaded with a new g-code for printing the sensing layer. After printing the PLA-CNT layer, the filament and nozzle were changed back to the initial setting and a thin layer of TPU with a thickness of 400 μm was printed on top of the substrate. For the cross-sensor, this procedure was repeated twice. The ends of the sensing layers were designed to be exposed to facilitate wire bonding.

SEM, Optical, and Thermal Characterization. The morphologies of the PLA-CNT filament and the 3D-printed sensor were characterized using a NanoSEM 230 field-emission scanning electron microscope (FE-SEM) with an accelerating voltage of 3.0 kV. The specimens that contained TPU were sputter-coated with a layer of platinum (thickness = 15 nm). Optical micrographs were taken with a ZEISS Axio Zoom V16 microscope. The thermal gravimetric analysis (TGA) measurement of the PLA-CNT filament was conducted in a Netzsch F3 Jupiter machine under a nitrogen atmosphere from 25 to 500 °C with a rate of 10 °C/min. The sample weight was around 10 mg. The differential scanning calorimetry (DSC) measurement of the PLA-CNT filament was performed using a PerkinElmer DSC 8000 machine from 30 to 200 °C with a rate of 10 °C/min. The sample weight was 8 mg, and it was placed inside a capped aluminum container with a hole on top.

Mechanical and Electromechanical Experiments. For the peel-off test, PLA-CNT was 3D-printed, sandwiched between TPU, and a paper tape was used to separate PLA-CNT and bottom TPU. The peel-off tests were performed with an ADMET eXpert 5951 fatigue testing machine. An Instron 3369 machine was used for all of the other tensile tests. For tensile tests, two wooden strips were bonded to one side of the sensors using the superglue and the strips were clamped to the Instron machine. For wire bonding, copper wires were attached to the sensors' surface using SPI Supplies silver paste and then covered with an aluminum tape. A Keysight 34465A digital multimeter and a Keysight E4980AL LCR meter were used to acquire the sensors' electrical resistance.

Fabrication of Sensorized Actuators. The four-armed actuator was 3D-printed with very low infill density of 10% to minimize the bending stress on the sensor. A separating TPU layer with a thickness of 0.4 mm was printed between the two sensor−conductor layers. After printing the sensors and conductors on this actuator, a solid TPU layer with a thickness of 1 mm was printed on top of them to completely encapsulate the sensing layer. For fabricating the testing fixtures, a PLA filament (blue, diameter: 1.75 mm) was purchased from Thinglab, Australia. The fixtures were 3D-printed with the same FDM machine and bonded to the actuator using LOCTITE superglue. The pneumatic actuator was 3D-printed using the same printer, and then, the sensor and conductors were printed on it.

Printing parameters are available in Table S7 in the Supporting Information.

ASSOCIATED CONTENT

Supporting Information

The Supporting Information is available free of charge at https://pubs.acs.org/doi/10.1021/acsami.9b21816.

Percolation threshold of the PLA-CNT filament, 3D printing parameters, infill analysis, noise analysis, peel-off test results, peel-off SEM characterization, and temperature-dependence test results (PDF)

Demonstration of the sensing mechanism (kissing-bond mechanism) in a 95% X-sensor under 2% tensile strain (MP4)

Three-dimensional printing of the 85% infill conductors on a four-armed actuator (MP4)

Three-dimensional printing of the 95% infill sensor on a four-armed actuator (MP4)

Demonstration of bending detection (upward) in a two-armed actuator gripper (MP4)

Demonstration of bending detection (downward) in a two-armed actuator gripper (MP4)

AUTHOR INFORMATION

Corresponding Author

Chun H. Wang — *School of Mechanical and Manufacturing Engineering, University of New South Wales, Sydney, NSW 2052, Australia;* orcid.org/0000-0001-6081-1487; Email: chun.h.wang@unsw.edu.au

Authors

Saeb Mousavi — *School of Mechanical and Manufacturing Engineering, University of New South Wales, Sydney, NSW 2052, Australia; The Robotics and Autonomous Systems Group, Commonwealth Scientific and Industrial Research Organization (CSIRO), Pullenvale 4069, Australia;* orcid.org/0000-0001-5821-3939

David Howard — *The Robotics and Autonomous Systems Group, Commonwealth Scientific and Industrial Research Organization (CSIRO), Pullenvale 4069, Australia*

Fenghua Zhang — *Center for Composite Materials and Structures, Harbin Institute of Technology, Harbin 150080, P. R. China*

Jinsong Leng — *Center for Composite Materials and Structures, Harbin Institute of Technology, Harbin 150080, P. R. China;* orcid.org/0000-0001-5098-9871

Complete contact information is available at:
https://pubs.acs.org/10.1021/acsami.9b21816

Author Contributions

S.M. initialized the concept; designed and fabricated the sensors, conductors, and sensor—actuator systems; designed and conducted the experiments; analyzed the data; and wrote the draft manuscript. D.H. supervised the work, wrote and revised the manuscript. F.Z. and J.L. fabricated the PLA-CNT filament and reviewed the manuscript. C.H.W. jointly initialized the concept, designed the experiments, supervised the work, and wrote and revised the manuscript.

Notes

The authors declare no competing financial interest.
All data needed to evaluate the results and conclusions in this paper are present in the paper or the Supporting Information.

REFERENCES

(1) Rus, D.; Tolley, M. T. Design, fabrication and control of soft robots. *Nature* **2015**, *521*, 467−475.

(2) Din, S.; Xu, W. L.; Cheng, L. K.; Dirven, S. A Stretchable Multimodal Sensor for Soft Robotic Applications. *IEEE Sens. J.* **2017**, *17*, 5678−5686.

(3) Park, J.; You, I.; Kim, T. Y.; Song, J.; Jeong, U. Ag nanowire-based transparent stretchable tactile sensor recognizing strain directions and pressure. *Nanotechnology* **2019**, *30*, No. 315502.

(4) Ridzuan, N. A. A.; Miki, N. Tooth-Inspired Tactile Sensor for Detection of Multidirectional Force. *Micromachines* **2019**, *10*, 18.

(5) Lee, H.; Kwon, D.; Cho, H.; Park, I.; Kim, J. Soft Nanocomposite Based Multi-point, Multi-directional Strain Mapping Sensor Using Anisotropic Electrical Impedance Tomography. *Sci. Rep.* **2017**, *7*, No. 39837.

(6) Chen, X. L.; Shao, J. Y.; Tian, H. M.; Li, X. M.; Tian, Y. Z.; Wang, C. Flexible three-axial tactile sensors with microstructure-enhanced piezoelectric effect and specially-arranged piezoelectric arrays. *Smart Mater. Struct.* **2018**, *27*, No. 025018.

(7) Jung, Y.; Lee, D. G.; Park, J.; Ko, H.; Lim, H. Piezoresistive Tactile Sensor Discriminating Multidirectional Forces. *Sensors* **2015**, *15*, 25463−25473.

(8) Sarwar, M. S.; Dobashi, Y.; Preston, C.; Wyss, J. K. M.; Mirabbasi, S.; Madden, J. D. W. Bend, stretch, and touch: Locating a finger on an actively deformed transparent sensor array. *Sci. Adv.* **2017**, *3*, No. e1602200.

(9) Pang, C.; Lee, G. Y.; Kim, T. I.; Kim, S. M.; Kim, H. N.; Ahn, S. H.; Suh, K. Y. A flexible and highly sensitive strain-gauge sensor using reversible interlocking of nanofibres. *Nat. Mater.* **2012**, *11*, 795−801.

(10) Park, J.; Kim, M.; Lee, Y.; Lee, H. S.; Ko, H. Fingertip skin−inspired microstructured ferroelectric skins discriminate static/dynamic pressure and temperature stimuli. *Sci. Adv.* **2015**, No. e1500661.

(11) Park, J.; Kim, J.; Hong, J.; Lee, H.; Lee, Y.; Cho, S.; Kim, S. W.; Kim, J. J.; Kim, S. Y.; Ko, H. Tailoring force sensitivity and selectivity by microstructure engineering of multidirectional electronic skins. *NPG Asia Mater.* **2018**, *10*, 163−176.

(12) Boutry, C. M.; Negre, M.; Jorda, M.; Vardoulis, O.; Chortos, A.; Khatib, O.; Bao, Z. N. A hierarchically patterned, bioinspired e-skin able to detect the direction of applied pressure for robotics. *Sci. Rob.* **2018**, *3*, No. eaau6914.

(13) Van Meerbeek, I. M.; De Sa, C. M.; Shepherd, R. F. Soft optoelectronic sensory foams with proprioception. *Sci. Rob.* **2018**, *3*, No. eaau2489.

(14) Farahani, R. D.; Dube, M.; Therriault, D. Three-Dimensional Printing of Multifunctional Nanocomposites: Manufacturing Techniques and Applications. *Adv. Mater.* **2016**, *28*, 5794−5821.

(15) Zhang, Y. F.; Zhang, N. B.; Hingorani, H.; Ding, N. Y.; Wang, D.; Yuan, C.; Zhang, B.; Gu, G. Y.; Ge, Q. Fast-Response, Stiffness-Tunable Soft Actuator by Hybrid Multimaterial 3D Printing. *Adv. Funct. Mater.* **2019**, *29*, No. 1806698.

(16) Wallin, T. J.; Pikul, J.; Shepherd, R. F. 3D printing of soft robotic systems. *Nat. Rev. Mater.* **2018**, *3*, 84−100.

(17) Guo, S.-Z.; Qiu, K. Y.; Meng, F. B.; Park, S. H.; McAlpine, M. C. 3D Printed Stretchable Tactile Sensors. *Adv. Mater.* **2017**, *29*, No. 1701218.

(18) Choi, J. W.; Emon, M. O. F.; Alkadi, F.; Lee, J.; Vatani, M. 3D printed stretchable tactile sensors *Abstr. Pap. Am. Chem. Soc.* 2016, 252.

(19) Delamare, J.; Sanders, R.; Krijnen, G. 3D Printed Biomimetic Whisker-Based Sensor with Co-planar Capacitive Sensing. *2016 IEEE Sens.* 2016, 1−3.

(20) Eijking, B.; Sanders, R.; Krijnen, G. Development of Whisker Inspired 3D Multi-Material Printed Flexible Tactile Sensors. *IEEE Sens.* 2017, 256−258.

(21) Lee, J.; Emon, M. O. F.; Vatani, M.; Choi, J. W. Effect of degree of crosslinking and polymerization of 3D printable polymer/ionic liquid composites on performance of stretchable piezoresistive sensors. *Smart Mater. Struct.* 2017, 26, No. 035043.

(22) Li, K.; Wei, H.; Liu, W. G.; Meng, H.; Zhang, P. X.; Yan, C. Y. 3D printed stretchable capacitive sensors for highly sensitive tactile and electrochemical sensing. *Nanotechnology* 2018, 29, No. 185501.

(23) Liu, L.; Huang, Y.; Li, F. Y.; Ma, Y.; Li, W. B.; Su, M.; Qian, X.; Ren, W. J.; Tang, K. L.; Song, Y. L. Spider-web inspired multi-resolution graphene tactile sensor. *Chem. Commun.* 2018, 54, 4810−4813.

(24) Qiu, K. Y.; Zhao, Z. C.; Haghiashtiani, G.; Guo, S. Z.; He, M. Y.; Su, R. T.; Zhu, Z. J.; Bhuiyan, D. B.; Murugan, P.; Meng, F. B.; Park, S. H.; Chu, C. C.; Ogle, B. M.; Saltzman, D. A.; Konety, B. R.; Sweet, R. M.; McAlpine, M. C. 3D Printed Organ Models with Physical Properties of Tissue and Integrated Sensors. *Adv. Mater. Technol.* 2018, 3, No. 1700235.

(25) Wang, Z. Y.; Gao, W. L.; Zhang, Q.; Zheng, K. Q.; Xu, J. W.; Xu, W.; Shang, E. W.; Jiang, J.; Zhang, J.; Liu, Y. 3D-Printed Graphene/Polydimethylsiloxane Composites for Stretchable and Strain-Insensitive Temperature Sensors. *ACS Appl. Mater. Interfaces* 2019, 11, 1344−1352.

(26) Wang, Z. Y.; Guan, X.; Huang, H. Y.; Wang, H. F.; Lin, W. E.; Peng, Z. C. Full 3D Printing of Stretchable Piezoresistive Sensor with Hierarchical Porosity and Multimodulus Architecture. *Adv. Funct. Mater.* 2019, 29, No. 1807569.

(27) Xie, M. Y.; Hisano, K.; Zhu, M. Z.; Toyoshi, T.; Pan, M.; Okada, S.; Tsutsumi, O.; Kawamura, S.; Bowen, C. Flexible Multifunctional Sensors for Wearable and Robotic Applications. *Adv. Mater. Technol.* 2019, 4, No. 1800626.

(28) Liu, C.; Huang, N. G.; Xu, F.; Tong, J. D.; Chen, Z. W.; Gui, X. C.; Fu, Y. L.; Lao, C. S. 3D Printing Technologies for Flexible Tactile Sensors toward Wearable Electronics and Electronic Skin. *Polymers* 2018, 10, 629.

(29) Christ, J. F.; Aliheidari, N.; Ameli, A.; Potschke, P. 3D printed highly elastic strain sensors of multiwalled carbon nanotube/thermoplastic polyurethane nanocomposites. *Mater. Des.* 2017, 131, 394−401.

(30) Kim, K.; Park, J.; Suh, J. H.; Kim, M.; Jeong, Y.; Park, I. 3D printing of multiaxial force sensors using carbon nanotube (CNT)/thermoplastic polyurethane (TPU) filaments. *Sens. Actuators, A* 2017, 263, 493−500.

(31) Christ, J. F.; Aliheidari, N.; Potschke, P.; Ameli, A. Bidirectional and Stretchable Piezoresistive Sensors Enabled by Multimaterial 3D Printing of Carbon Nanotube/Thermoplastic Polyurethane Nanocomposites. *Polymers* 2018, 11, 11.

(32) Gul, J. Z.; Sajid, M.; Choi, K. H. 3D printed highly flexible strain sensor based on TPU-graphene composite for feedback from high speed robotic applications. *J. Mater. Chem. C* 2019, 7, 4692−4701.

(33) Mousavi, S.; Howard, D.; Wu, S.; Wang, C. *An ultrasensitive 3D printed tactile sensor for soft robotics*, arXiv:1601.03346. arXiv.org e-Print archive. https://arxiv.org/abs/1810.09236 (accessed Sep 24, 2018).

(34) Lee, J. I.; Eun, Y.; Choi, J.; Kwon, D. S.; Kim, J. Using Confined Self-Adjusting Carbon Nanotube Arrays as High-Sensitivity Displacement Sensing Element. *ACS Appl. Mater. Interfaces* 2014, 6, 10181−10187.

(35) Tas, M. O.; Baker, M. A.; Masteghin, M. G.; Bentz, J.; Boxshal, K.; Stolojan, V. Highly Stretchable, Directionally Oriented Carbon Nanotube/PDMS Conductive Films with Enhanced Sensitivity as Wearable Strain Sensors. *ACS Appl. Mater. Interfaces* 2019, 11, 39560−39573.

(36) Chen, S.; Song, Y. J.; Ding, D. Y.; Ling, Z.; Xu, F. Flexible and Anisotropic Strain Sensor Based on Carbonized Crepe Paper with Aligned Cellulose Fibers. *Adv. Funct. Mater.* 2018, 28, No. 1802547.

(37) Huang, S.; He, G.; Yang, C.; Wu, J. M.; Guo, C.; Hang, T.; Li, B. H.; Yang, C. D.; Liu, D.; Chen, H. J.; Wu, Q. N.; Gui, X. C.; Deng, S. Z.; Zhang, Y.; Liu, F. M.; Xie, X. Stretchable Strain Vector Sensor Based on Parallelly Aligned Vertical Graphene. *ACS Appl. Mater. Interfaces* 2019, 11, 1294−1302.

(38) Sui, C.; Yang, Y. C.; Headrick, R. J.; Pan, Z. X.; Wu, J. Y.; Zhang, J.; Jia, S.; Li, X. W.; Gao, W. L.; Dewey, O. S.; Wang, C.; He, X. D.; Kono, J.; Pasquali, M.; Lou, J. Directional sensing based on flexible aligned carbon nanotube film nanocomposites. *Nanoscale* 2018, 10, 14938−14946.

(39) Lee, J.-H.; Kim, J.; Liu, D.; Guo, F.; Shen, X.; Zheng, Q.; Jeon, S.; Kim, J.-K. Highly Aligned, Anisotropic Carbon Nanofiber Films for Multidirectional Strain Sensors with Exceptional Selectivity. *Adv. Funct. Mater.* 2019, 29, No. 1901623.

(40) Chen, H. T.; Su, Z. M.; Song, Y.; Cheng, X. L.; Chen, X. X.; Meng, B.; Song, Z. J.; Chen, D. M.; Zhang, H. X. Omnidirectional Bending and Pressure Sensor Based on Stretchable CNT-PU Sponge. *Adv. Funct. Mater.* 2017, 27, No. 1604434.

(41) Mu, C. H.; Song, Y. Q.; Huang, W. T.; Ran, A.; Sun, R. J.; Xie, W. H.; Zhang, H. W. Flexible Normal-Tangential Force Sensor with Opposite Resistance Responding for Highly Sensitive Artificial Skin. *Adv. Funct. Mater.* 2018, 28, No. 1707503.

(42) Khang, D. Y.; Jiang, H. Q.; Huang, Y.; Rogers, J. A. A stretchable form of single-crystal silicon for high-performance electronics on rubber substrates. *Science* 2006, 311, 208−212.

(43) Rogers, J. A.; Someya, T.; Huang, Y. G. Materials and Mechanics for Stretchable Electronics. *Science* 2010, 327, 1603−1607.

(44) Li, K.; Cheng, X.; Zhu, F.; Li, L. Z.; Xie, Z. Q.; Luan, H. W.; Wang, Z. H.; Ji, Z. Y.; Wang, H. L.; Liu, F.; Xue, Y. G.; Jiang, C. Q.; Feng, X.; Li, L. M.; Rogers, J. A.; Huang, Y. G.; Zhang, Y. H. A Generic Soft Encapsulation Strategy for Stretchable Electronics. *Adv. Funct. Mater.* 2019, 29, No. 1806630.

(45) Byun, S.-H.; Sim, J. Y.; Zhou, Z.; Lee, J.; Qazi, R.; Walicki, M. C.; Parker, K. E.; Haney, M. P.; Choi, S. H.; Shon, A.; Gereau, G. B.; Bilbily, J.; Li, S.; Liu, Y.; Yeo, W.-H.; McCall, J. G.; Xiao, J.; Jeong, J.-W. Mechanically transformative electronics, sensors, and implantable devices. *Sci. Adv.* 2019, 5, No. eaay0418.

(46) Ha, S. H.; Ha, S. H.; Jeon, M. B.; Cho, J. H.; Kim, J. M. Highly sensitive and selective multidimensional resistive strain sensors based on a stiffness-variant stretchable substrate. *Nanoscale* 2018, 10, 5105−5113.

(47) Murty, Y. V. Electrical and Electronic Connectors: Materials and Technology. In *Encyclopedia of Materials: Science and Technology*; Buschow, K. H. J.; Cahn, R. W.; Flemings, M. C.; Ilschner, B.; Kramer, E. J.; Mahajan, S.; Veyssière, P., Eds.; Elsevier, 2001; pp 2483−2494.

(48) Laschi, C.; Mazzolai, B.; Cianchetti, M. Soft robotics: Technologies and systems pushing the boundaries of robot abilities. *Sci. Rob.* 2016, 1, No. eaah3690.

(49) Wang, H. B.; Totaro, M.; Beccai, L. Toward Perceptive Soft Robots: Progress and Challenges. *Adv. Sci.* 2018, 5, No. 1800541.

(50) Helbling, T.; Roman, C.; Hierold, C. Signal-to-Noise Ratio in Carbon Nanotube Electromechanical Piezoresistive Sensors. *Nano Lett.* 2010, 10, 3350−3354.

(51) Pang, C.; Koo, J. H.; Nguyen, A.; Caves, J. M.; Kim, M. G.; Chortos, A.; Kim, K.; Wang, P. J.; Tok, J. B. H.; Bao, Z. A. Highly Skin-Conformal Microhairy Sensor for Pulse Signal Amplification. *Adv. Mater.* 2015, 27, 634−640.

(52) Peng, S. H.; Blanloeuil, P.; Wu, S. Y.; Wang, C. H. Rational Design of Ultrasensitive Pressure Sensors by Tailoring Microscopic Features. *Adv. Mater. Interfaces* 2018, 5, No. 1800403.

(53) Zhang, J.; Zhao, Y.; Ge, Y. X.; Li, M.; Yang, L. J.; Mao, X. L. Design Optimization and Fabrication of High-Sensitivity SOI

Pressure Sensors with High Signal-to-Noise Ratios Based on Silicon Nanowire Piezoresistors. *Micromachines* **2016**, *7*, 187.

(54) Liu, Y.; Zhang, W.; Zhang, F. H.; Leng, J. S.; Pei, S. P.; Wang, L. Y.; Jia, X. Q.; Cotton, C.; Sun, B. Z.; Chou, T. W. Microstructural design for enhanced shape memory behavior of 4D printed composites based on carbon nanotube/polylactic acid filament. *Compos. Sci. Technol.* **2019**, *181*, No. 107692.

(55) Zhang, F. H.; Wang, L. L.; Zheng, Z. C.; Liu, Y. J.; Leng, J. S. Magnetic programming of 4D printed shape memory composite structures. *Composites, Part A* **2019**, *125*, No. 105571.